Neon Matrix ESR and CI Theoretical Investigation of AlF^+; Photoionization of AlF from Thermal and Laser Sputtering Generation Methods

Lon B. Knight, Jr.,*† Edward Earl,† A. R. Ligon,† D. P. Cobranchi,† J. R. Woodward,† J. M. Bostick,† E. R. Davidson,‡ and David Feller‡

Contribution from the Chemistry Department, Furman University, Greenville, South Carolina 29613, and the Department of Chemistry, Indiana University, Bloomington, Indiana 47405. *Received February 27, 1986*

Abstract: The high-temperature AlF^+ radical cation has been generated by the photoionization of AlF(g) produced both by a laser sputtering method and high-temperature vaporization reactions. This represents the first spectroscopic study of AlF^+ and establishes its ground electronic state as $^2\Sigma$. The ESR spectrum of the AlF^+ radical, isolated in a neon matrix at 4 K, has been analyzed in detail, and the experimental magnetic parameters obtained show excellent agreement with the results of an extensive ab initio theoretical calculation. The AlF^+ magnetic parameters in a neon matrix are the following: $g_\parallel$ = 2.0015 (5), $g_\perp$ = 2.0000 (5); Al, $A_\parallel$ = 2893 (8) MHz, $A_\perp$ = 2782 (6) MHz, ^{19}F, $A_\parallel$ = 473 (5) MHz, $A_\perp$ = 90 (5) MHz. The electronic structure of AlF^+ is compared to the isoelectronic series $^{29}SiO^+$, AlO, and MgF utilizing both experimental and theoretical findings. Orbital populations for the unpaired electron were obtained from the commonly applied free atom comparison method (FACM) and from a Mulliken type population analysis of a CI wave function which yielded magnetic parameters in close agreement with experiment. The effect of "core–other valence overlap" was studied in detail for this isoelectronic series. This AlF^+ study and a previous one for SiO^+ are apparently the first ESR investigations of high-temperature inorganic cation radicals.

Generation and trapping techniques have been developed to permit the ESR (electron spin resonance) investigation of small, highly reactive cations having relatively large electron affinities in neon matrices near 4 K. Examples of cations recently studied by ESR with these neon matrix trapping techniques include CO^+,[1] NH_3^+,[1] N_2^+,[2] H_2O^+,[3] H_2CO^+,[4] Cd^+,[5] CH_4^+,[6] $C_2O_2^+$,[7] and the high-temperature cation radical $^{29}SiO^+$.[8] Experimental results have also been obtained for a few anion radicals trapped in neon matrices as free ions including F_2^-,[9] HF^-,[10] DF^-,[10] Cl_2^-,[10] and HCl^-.[10] The Cl_2^- and HCl^- radicals have been previously studied by ESR as chemically bonded ion pairs, M^+X^-, in argon matrices.[11,12] The inert nature of the neon host, its low polarizability, and large ionization energy (21.6 eV) allow free or gas-like properties of ions to be obtained. Cations having electron affinities much greater than 10–11 eV apparently cannot be stabilized in other matrix materials such as argon or freon matrices. Paramagnetic ions trapped in frozen ionic solutions or crystalline hosts can be highly perturbed, and the information obtained might not accurately represent the inherent properties of the trapped species.

This AlF^+ study illustrates that the matrix isolation trapping method could be applied to a wide range of charged and neutral chemical systems produced by reactive laser sputtering processes. The reactive intermediates produced by such laser induced gas–surface reactions could be characterized by the wide range of spectroscopic methods currently used with the matrix isolation technique. Current research efforts in our laboratory are using this laser technique to produce metal nitride neutral and cation radicals for ESR matrix studies. The feasibility of combining high-temperature vaporization and various ion generation techniques with the neon matrix isolation method for ESR spectroscopy has been demonstrated in a recent report on[28,29] SiO^+ which was the first high-temperature (>1000 K) cation radical studied by ESR with any experimental approach.[8] Many high-temperature neutral radicals have been investigated via the ESR matrix method, and the results have been presented in a recent monograph on the subject.[13] This AlF^+ study, which also utilizes high-temperature vaporization, extends the experimental capabilities to laser sputtering generation of the desired neutral species (AlF).

Vibrational studies of AlF in neon, argon, and krypton matrices were reported in earlier work.[14] High-temperature vaporization reduction reactions were used to generate AlF for the matrix IR studies as well as mass spectrometric measurements which yielded an appearance potential for AlF of 9.7 eV.[15] Lide has presented a brief account on the discovery of AlF and has reported an experimental value for the dipole moment of 1.53 D for the neutral diatomic.[16]

ESR measurements on AlF^+ are especially interesting since it is isoelectronic to AlO,[17] MgF,[18] and SiO^+.[8] The ^{19}F hfs of AlF^+ is highly anisotropic, and the extremely large ^{27}Al hfs, the largest reported for any Al radical, necessitated the use of an exact diagonalization treatment for extracting the magnetic parameters from the observed ESR lines which extended over the magnetic field range of approximately 200–6000 G at the X-band microwave frequency. ESR results for this series of "simple" diatomic radicals permit the effect of charge on the electronic structure to be analyzed by comparison of the various nuclear hyperfine parameters

† Furman University.
‡ Indiana University.

(1) (a) Knight, L. B., Jr.; Steadman, J. *J. Chem. Phys.* **1982**, *77*, 1750. (b) Knight, L. B., Jr.; Steadman, J. *J. Am. Chem. Soc.* **1984**, *106*, 900.
(2) Knight, L. B., Jr.; Bostick, J. M.; Woodward, R. J.; Steadman, J. *J. Chem. Phys.* **1983**, *78*, 6415.
(3) Knight, L. B., Jr.; Steadman, J. *J. Chem. Phys.* **1983**, *78*, 5940.
(4) Knight, L. B., Jr.; Steadman, J. *J. Chem. Phys.* **1984**, *80*, 1018.
(5) Knight, L. B., Jr.; Miller, P. K.; Steadman, J. *J. Chem. Phys.* **1984**, *80*, 4587.
(6) Knight, L. B., Jr.; Steadman, J.; Feller, D.; Davidson, E. R. *J. Am. Chem. Soc.* **1984**, *106*, 3700.
(7) Knight, L. B., Jr.; Steadman, J.; Miller, P. K.; Bowman, D. E.; Davidson, E. R.; Feller, D. *J. Chem. Phys.* **1984**, *80*, 4593.
(8) Knight, L. B., Jr.; Ligon, A.; Woodward, R. W.; Feller, D.; Davidson, E. R. *J. Am. Chem. Soc.* **1985**, *107*, 2857.
(9) Knight, L. B., Jr.; Earl, E.; Ligon, A. R.; Cobranchi, D. P. *J. Chem. Phys.*, in press.
(10) Knight, L. B., Jr.; Cobranchi, D. P.; Ligon, A. R., to be published.
(11) Martinez de Pinillos, J. V.; Weltner, W., Jr. *J. Chem. Phys.* **1976**, *65*, 4256.
(12) Lindsay, D. M.; Symons, M. C. R.; Herschbach, D. R.; Kwiram, A. L. *J. Phys. Chem.* **1982**, *86*, 3789.
(13) Weltner, W., Jr. *Magnetic Atoms and Molecules*; Van Nostrand-Reinhold Co., Inc.: New York, 1983.
(14) Snelson, A. *J. Phys. Chem.* **1967**, *71*, 3202.
(15) Blue, G. D.; Green, J. W.; Bautista, R. G.; Margrave, J. L. *J. Phys. Chem.* **1963**, *67*, 877. Porter, R. F. *J. Chem. Phys.* **1960**, *33*, 951.
(16) Lide, D. R., Jr. *J. Chem. Phys.* **1965**, *42*, 1013.
(17) Knight, L. B., Jr.; Weltner, W., Jr. *J. Chem. Phys.* **1971**, *55*, 5066.
(18) Knight, L. B., Jr.; Easley, W. C.; Weltner, W., Jr.; Wilson, M. *J. Chem. Phys.* **1971**, *54*, 322.

0002-7863/86/1508-5065$01.50/0

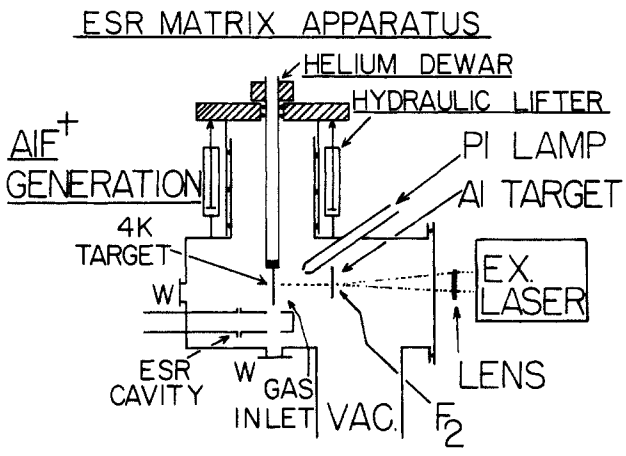

Figure 1. ESR matrix apparatus used for generating AlF from laser sputtering an aluminum target under F_2(g) flow conditions. AlF^+ is formed during neon deposition by photoionization from the open-ended neon resonance lamp (16.8 eV) labeled "PI".

which directly reflect the amount of "s" and "p" character for the odd electron. No previous spectroscopic studies of any kind have been reported for AlF^+, and theory shows that it possesses the same $(^2\Sigma)1\sigma^2 2\sigma^2 3\sigma^2 4\sigma^2 5\sigma^2 6\sigma^2 7\sigma^1 1\pi^4 2\pi^4$ electronic ground state as the AlO and SiO^+ radicals whose hyperfine spin properties have previously been studied with use of ab initio techniques.[8,19] Hartree–Fock (HF) spin densities for AlO and SiO^+ have been shown to be grossly incorrect. In fact, in the case of AlO two solutions of the HF equations, with very different unpaired spin distributions, have been reported.[19] While full configuration interaction (CI) yields properties which are invariant with respect to the choice of orbitals, in practice even large multireference single and double excitation CI (MR SD–CI) proved unable to completely overcome the SCF induced bias in the wave function. A redefinition of the molecular orbitals by means of either a multiconfiguration SCF (MCSCF) or iterative natural orbital (INO) procedure[20] was found to be necessary in order to obtain agreement to within 5% of experiment. The best theoretical isotropic numbers were uniformly too small in absolute magnitude. For example, the theoretical silicon isotropic hyperfine value in SiO^+ was −769 MHz compared with an experimental value of −798 MHz. The aluminum isotropic values in AlO were 705 MHz (theory) and 767 MHz (experiment).

Klein and Rosmus[21] have recently published calculations on AlF^+ using a pseudonatural orbital CI (PNO–CI) with the coupled electron pair approximation (CEPA). They reported an optimized bond length of 1.601 Å and an origin dependent dipole moment of 2.28 D with Al at the center of the coordinate system and F at $-R$ along the z axis. The positive sign of the dipole moment indicates that the moment of positive charge is greater around Al than is the moment of negative charge.

Experimental Section

The hydraulic ESR cryostat and computer interfaced spectrometer used for these AlF^+ neon matrix isolation experiments have been described in previous reports.[1,2,5] A modified liquid helium Heli-Tran cryostat (Air Products) was used to cool a thin copper matrix deposition target to approxiately 4 K.

The electron bombardment ion generation procedure used in combination with a high-temperature Knudsen effusion oven was described in the N_2^+ report, and the open tube neon discharge photoionization source in combination with a high-temperature oven was described in the CO^+ and SiO^+ studies. AlF^+ was generated by both the electron bombardment and photoionization methods by using two different sources of neutral AlF-laser sputtering and high-temperature (>1000 K) vaporization–reduction reactions of AlF_3(s). The KrF excimer laser (Lumonics) sputtering technique developed for these ESR matrix studies was found to produce "cleaner" and more intense ESR spectra of AlF^+ than the conventional high-temperature source.

Figure 1 presents a schematic of the experimental arrangement used to produce neon-isolated AlF^+ by photoionization of AlF(g) generated by the laser sputtering of aluminum metal under F_2(g) flow conditions. The 16.8 eV open tube neon resonance photoionization source powered by a microwave generator is denoted "PI" in Figure 1, and "W" indicates the position of quartz windows in the ESR cryostat. Neon matrix samples were prepared in the following manner. Neon gas (Matheson research grade) was passed through a 5 Å molecular sieve trap cooled to 77 K and directed toward the matrix target at a flow rate of 5.0 SCCM. The 9 mm (o.d.) neon resonance lamp whose open end was located 5 cm from the deposition target was operated at 60 W forward and 2 W reflected power with a continuous neon flow of 3.0 SCCM. Background pressure in the apparatus of 5×10^{-7} Torr typically increased to $\approx 8 \times 10^{-5}$ Torr under gas flow conditions. Mounted 8 cm from the deposition surface was an aluminum foil target (2 cm × 1 cm × 0.25 mm). See Figure 1. Output from the KrF laser (249 nm; 200 mJ and 10 Hz repetition rate) was focused to a spot size of about 1 mm on the backside of the Al target relative to the matrix deposition surface. Fluorine gas was also directed toward the backside of the Al target by a passivated copper tube. An X–Y translator was used to move the laser focusing lens (fl = 38 cm) so that the laser spot on the aluminum target could be conveniently moved over the aluminum surface. The flow rate of the high-purity oxygen-free F_2(g) (obtained from the Argonne National Laboratory) was approximately 10^{-3} times that of the neon matrix gas flow rate. The focused laser created a small hole in the aluminum target after about 3 s, and as the hole continued to expand AlF(g) was apparently sputtered forward where it was photoionized by the neon resonance lamp during the matrix deposition process. To increase the time that AlF(g) was sputtered forward, the laser focusing lens was carefully moved to direct the beam around the edges of the laser created hole. The laser beam could also be moved to a fresh position on the aluminum target and the reactive sputtering process repeated until sufficient AlF^+ had been trapped for ESR detection. Typically, the laser hole burning sputtering process had to be sustained for approximately 20 min, producing about 15 different holes in order to trap sufficient amounts of AlF^+ for ESR study. The laser sputtering process alone did not produce AlF^+. This was determined by conducting the same deposition sputtering experiment without having the neon resonance lamp operating.

Another independent method of generating AlF(g) involved the high-temperature vaporization reduction reaction of AlF_3(s) plus Al(s) conducted at 1100 K and AlF_3(s) plus Ca(s) at 1000 K. These separate high-temperature reactions were conducted in resistively heated tantalum effusion ovens and have been shown to produce AlF(g) by direct mass spectrometric measurements and matrix isolation trapping experiments employing infrared vibrational assignments.[14] In the early stages of these ESR matrix experiments designed to produce AlF^+ we repeated the matrix IR experiments to ascertain that proper experimental conditions had been established for the generation of AlF(g). The vibrational frequencies observed agreed within ± 1 cm^{-1} with those reported earlier for AlF in argon matrices.[14] A Perkin-Elmer Model 580 was used to record the IR spectra, and the various reagents (AlF_3, Al, Ca) were the highest purities available from Alfa Ventron. The high-temperature flange containing the Knudsen cell with its chemical charge used for these IR matrix studies was transferred to the high-temperature furnace section of the ESR matrix apparatus. Exactly the same vaporization conditions were repeated in the ESR apparatus with the same Knudsen cell. The major differences were that neon matrices were formed with the neon resonance photoionization lamp operating during deposition and the trapping surface was copper rather than the CsI window employed in the IR matrix apparatus.

Results

ESR Spectral Analysis of AlF^+. Neon matrix deposition of AlF(g) from either the laser or high-temperature source under ionizing conditions (either electron bombardment or photoionization) produced the same ESR spectra that consisted of a sextet of doublets for both the perpendicular ($\theta = 90°$) and parallel ($\theta = 0°$) directions. This is the expected pattern for AlF^+ since $I = {}^5/_2$ for ^{27}Al and $I = {}^1/_2$ for ^{19}F. The large amount of ^{19}F A tensor anisotropy caused "extra" or off-angle features that for some transitions were more intense than the usually dominant $\theta = 90°$ lines where θ is the angle between the applied magnetic field and the molecular symmetry axis of AlF^+.

Given the extremely large magnitude of the Al hfs, $A_\perp = 994$ (2) G, the various ESR transitions extended from 323 to 5770 G for the X-band microwave frequency of 9570 MHz. Second-order approximations are not appropriate for such large hfs, and

(19) Knight, L. B., Jr.; Wise, M. B.; Davidson, E. R.; McMurchie, L. E. *J. Chem. Phys.* **1982**, *76*, 126.
(20) Bender, C. F.; Davidson, E. R. *J. Phys. Chem.* **1966**, *70*, 2675.
(21) Klein, R.; Rosmus, P. *Theor. Chim. Acta (Berlin)* **1984**, *66*, 21.

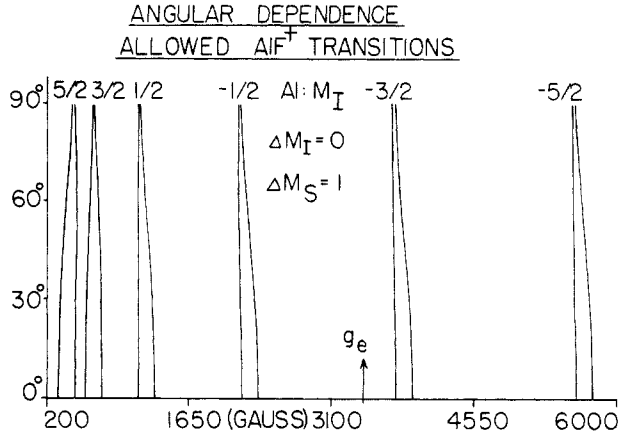

Figure 2. Angular dependence of the allowed ESR hyperfine lines of AlF^+ obtained from an exact diagonalization treatment is shown by using the magnetic parameters listed in Tables I and II for a neon matrix sample. The angle plotted (θ) is the angle between the molecular axis of AlF^+ and the applied magnetic field. The field position corresponding to the free spin value is denoted by g_e. See Figure 3.

an exact diagonalization treatment of the following axially symmetric spin Hamiltonian had to be used to extract the magnetic parameters from the observed ESR line positions listed in Table I. The inclusion of nuclear Zeeman and ^{27}Al quadrupole terms

$$\hat{H} = g_\parallel \beta H_z S_z + g_\perp \beta (H_x S_x + H_y S_y) + [A_\parallel S_z I_z + A_\perp (I_x S_x + I_y S_y)]_F + [A_\parallel S_z I_z + A_\perp (I_x S_x + I_y S_y)]_{Al}$$

did not affect the excellent agreement between calculated and observed lines for quadrupole coupling constants in the range predicted by the ab initio CI calculations. See Table IV.

The resulting 24 × 24 spin energy determinants were solved as a function of θ and the applied magnetic field for a given set of input parameters with the assistance of various quadratic interpolation schemes whose accuracy was checked at numerous specific points. The 24 θ-dependent magnetic energy levels obtained from these determinants were combined in all reasonable combinations and weighted according to calculated transition probabilities. These angular and field-dependent transitions were then coupled to a first derivative Lorentzian line shape function for direct comparison with the experimental ESR spectra. To assist in the assignment of off-angle or extra transitions, θ vs. H_{RES} plots were also generated from the diagonalization process. As shown by the data in Table I, all of the expected ESR lines were observed, and their positions, phases, and relative intensities exhibited agreement with the calculated positions well within the experimental uncertainties. Figures 2 and 3 present the overall spectral characteristics of AlF^+, showing line positions, θ vs. H_{RES} dependencies, and simulated first derivative spectra of all transitions. Figures 4–6 present various spectral regions in a more expanded scale format where direct comparison between simulated and experimental spectra are made. The lowest field transitions

Table I. Observed and Calculated ESR Line Positions for AlF^+ in Neon Matrix at 4 K

		θ = 0° lines (parallel)		θ = 90° lines (perpendicular)	
		obsd[a]	calcd[b]	obsd[a]	calcd[b]
Al	$M_I = {}^5/_2$				
F	$M_I = {}^1/_2$	323 (2)	323	469 (1)	469
	$M_I = -{}^1/_2$	490 (2)	490	490 (1)	492
	Note: strong off-angle (59 ± 5°) feature observed 513 (1); calcd 513				
Al	$M_I = {}^3/_2$				
F	$M_I = {}^1/_2$	604	603	678 (2)	678
	$M_I = -{}^1/_2$	773 (3)	769	690 (3)	693
Al	$M_I = {}^1/_2$				
F	$M_I = {}^1/_2$	1148 (3)	1145	1141 (3)[c]	1144
	$M_I = -{}^1/_2$	1314 (3)	1311	1159 (3)	1162
Al	$M_I = -{}^1/_2$				
F	$M_I = {}^1/_2$	2203 (3)	2200	*d*	2160
	$M_I = -{}^1/_2$	2371 (3)	2368	2182 (3)	2185
Al	$M_I = -{}^3/_2$				
F	$M_I = {}^1/_2$	3770 (3)	3768	*e*	3727
	$M_I = -{}^1/_2$	3939 (3)	3937	3756 (1)	3757
Al	$M_I = -{}^5/_2$				
F	$M_I = {}^1/_2$	5601 (2)	5600	f	5559
	$M_I = -{}^1_2$	5770 (2)	5769	5592 (1)	5591

[a] All observed line positions in gauss for a microwave frequency of 9569.5 (3) MHz. [b] All calculated line positions in gauss were obtained from an exact diagonalization analysis using the g and A values listed in Table II. See text. [c] Note: strong off-angle (69 ± 5°) feature observed and calculated at 1132 (2) G partially obscures this perpendicular line. [d] Note: strong off-angle (74 ± 3°) feature observed and calculated at 2156 obscures this perpendicular line. [e] Note: strong off-angle (74 ± 3°) feature observed at 3722 (1) and calculated at 3722 obscures this perpendicular line. [f] Note: strong off-angle (72 ± 3°) feature observed at 5556 (1) and calculated at 5557 obscures this perpendicular line.

(Al: $M_I = {}^5/_2$ and $^3/_2$) in the 300–800-G region are shown in Figure 4B and compared with simulated spectra in Figure 4A. The dashed lines superimposed over Figure 4A give the θ vs. H_{RES} dependence of these two hyperfine transitions. Note that for the $M_I = {}^5/_2$ transition, the most intense feature occurs not at θ = 90° but at the intermediate angle of approximately 59° for the higher field component of the ^{19}F doublet (^{19}F: $M_I = -{}^1/_2$). The lower field ^{19}F component ($M_I = {}^1/_2$) for this $M_I = {}^5/_2$ Al transition does not have an infinite slope at any intermediate angle along the θ vs. H_{RES} curve. Thus no "extra" or off-angle features are predicted nor observed in this spectral region. Neither of the ^{19}F components of the Al $M_I = {}^3/_2$ transition show extra features, and the spectrum in this region exhibits a classical line shape and phase pattern with observed lines occurring at the θ = 0° and 90° limits. A and B in Figure 5 present a similar comparison between simulated and observed spectra for the Al $M_I = {}^1/_2$ transition.

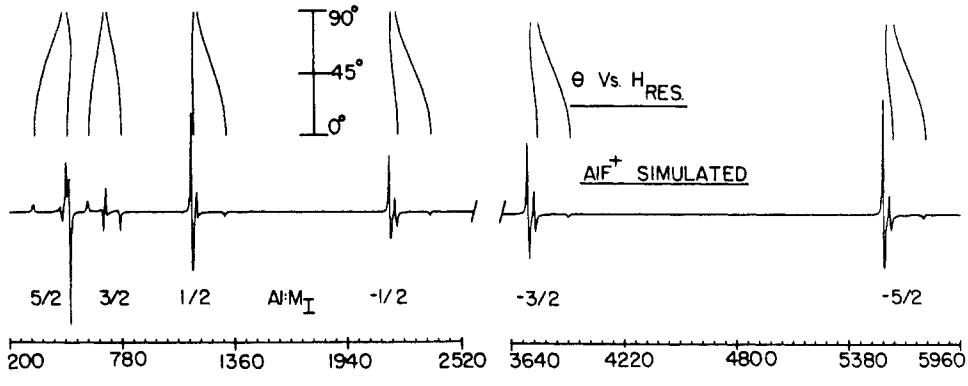

Figure 3. The computer simulated first derivative ESR spectrum for a powder sample of AlF^+ is shown for all allowed hyperfine transitions. On the same magnetic scale above each transition is presented the θ vs. H_{RES} dependence. See Figures 4–6 for expanded scale presentations of various spectral regions. The magnetic field for g_e is 3420 G and the magnetic parameters employed are listed in Tables I and II.

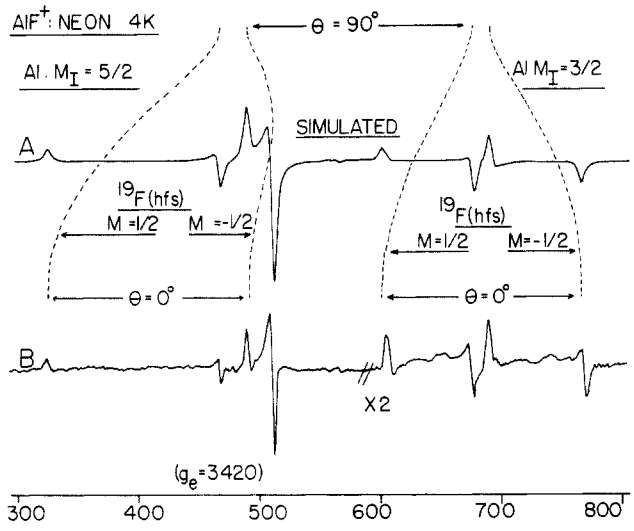

Figure 4. Simulated (A) and experimental (B) first derivative ESR spectra of AlF^+ in neon matrix at 4 K for the two lowest field Al hyperfine lines are shown. The dashed curves superimposed over the simulated spectrum show the θ vs. H_{RES} dependence. Note that the higher field ^{19}F ($M_I = -1/2$) component of the Al $M_I = 5/2$ transition exhibits a pronounced off-angle line at $\theta \approx 59°$ which is the most prominent feature for this entire spectral region. See Table I for exact line positions and magnetic parameters employed.

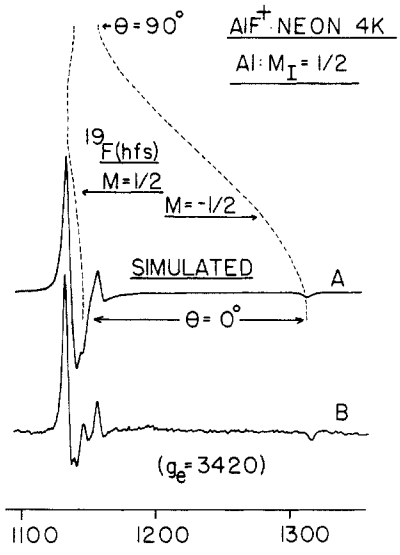

Figure 5. Simulated (A) and experimental (B) ESR spectra of AlF^+ in neon matrix for the Al $M_I = 1/2$ transition is presented. The dashed curves show the θ vs. H_{RES} dependence. An intense off-angle line is observed for the lower field ^{19}F component that overlaps the normally dominant $\theta = 90°$ (perpendicular transition). See Figure 4 and Table I for exact line positions and magnetic parameters employed.

As indicated in Table I, the exact position of the perpendicular transition ($\theta = 90°$) for the low-field (^{19}F: $M_I = 1/2$) component is obscured by the intense off-angle feature at $\theta = 69°$. The highest field transition, Al $M_I = -5/2$, is shown in Figure 6B and compared with a simulated spectrum in Figure 6A. Again the exact position of the $\theta = 90°$ transition for ^{19}F $M_I = 1/2$ is obscured by a strong off-angle feature. For all of the six major spectral regions, the six M_I values for Al, the agreement between observed and simulated spectra using the magnetic parameters given in Table I is excellent in every detail. However, the spectra recorded on the first set of experiments was difficult to recognize since it does deviate considerably from an obvious sextet of equally intense doublets for the parallel and perpendicular lines. Also, higher order effects cause the internal ^{19}F doublet splittings for the six Al transitions to be unequal. Without access to exact simulated spectra and θ vs. H_{RES} results for comparative purposes, it would have been impossible to assign the ESR spectral details of AlF^+

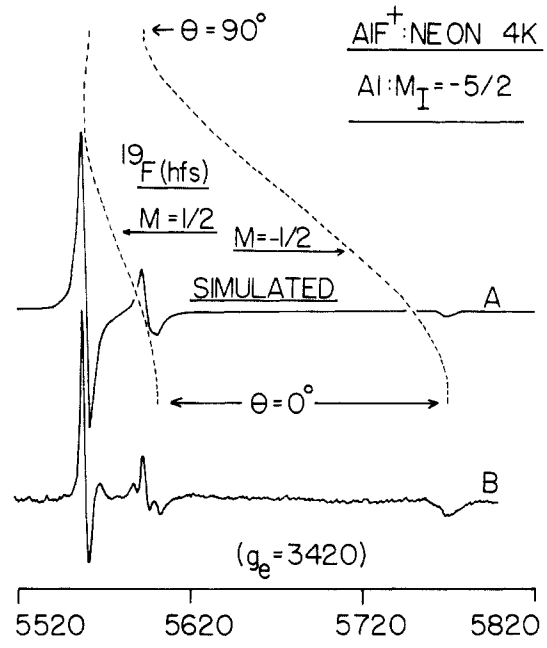

Figure 6. Simulated (A) and experimental (B) ESR spectra of AlF^+ in neon matrix for the Al $M_I = -5/2$ transition is shown. Dashed curves give the θ vs. H_{RES} dependence. An intense off-angle feature on the lower field ^{19}F component overlaps the $\theta = 90°$ perpendicular transition. See Table I for exact line positions and magnetic parameters employed.

and extract accurate magnetic parameters.

Laser Sputtering. The laser sputtering method developed for these matrix experiments was originally tried for the purpose of generating a cleaner source of AlF(g) for subsequent photoionization. The thermal method of AlF(g) generation employing AlF_3(s) produced an impurity species discussed below that made the AlF^+ ESR spectral assignment especially difficult. The laser method produced only the AlF^+ radical (in addition to trace amounts of normally observed impurities such as CH_3, HCO, N, and H atoms) whose magnetic parameters obtained from the ESR spectra show excellent agreement with ab initio CI calculations.

The major "trial and error" phase of the laser sputtering experiment was to find a geometrical arrangement for the aluminum target such that reflected UV laser radiation would not strike the neon matrix deposition sample. Experiments with previously studied ions such as H_2O^+ and N_2^+ demonstrated that only a few pulses of such UV light were sufficient to photobleach nearly all cation radicals. The photobleaching process has been described previously for ESR, electronic, and vibrational matrix studies of charged species.[1,22,23] Apparently, electrons are photoionized from the anion traps in the matrix and travel throughout the lattice neutralizing cations. The spectra of most neutral species are not affected, and hence the photobleaching process can be a useful technique in distinguishing between charged and uncharged matrix isolated species. To prevent photobleaching an arrangement was finally found that allowed laser sputtered species to impinge on the matrix deposition target without the reflected laser radiation. The hole burning reactive sputtering process that was successful has been described in the Experimental Section. It was necessary to locate the matrix deposition target slightly off the line defined by the laser beam. Apparently the molecules that were laser sputtered off the opposite side (matrix side) once a hole formed vaporized over a relatively large solid angle and could strike the off-line matrix target. The laser light traveled more directly through the hole and hence did not strike the matrix target. In this arrangement sputtered molecules could be matrix isolated without the deleterious photobleaching effect of direct or reflected laser radiation striking the deposited matrix sample. As the laser sputtered AlF(g) was being deposited in the neon matrix, con-

(22) Andrews, L. *Annu. Rev. Phys. Chem.* **1979**, *30*, 89.
(23) Bondybey, V. E.; English, J. H. *J. Chem. Phys.* **1979**, *71*, 777.

Table II. Magnetic and Electronic Structure Comparisons of AlF^+ with Other Isoelectronic $^2\Sigma$ Radicals; 4 K Neon Matrix Data

								% "s"[b]		% "p"[b]		
		$g_\parallel$	$g_\perp$	$A_\parallel$[a]	$A_\perp$[a]	A_{iso}[a]	A_{dip}[a]	neutral Al[c]	Al^{2+}[d]	neutral Al[c]	Al^{2+}[e]	Al^{2+}[f]
AlF^+	(Al)	2.0015 (5)	2.0000 (5)	2893 (8)	2782 (6)	2819 (6)	37 (5)	(72)	61	(44)	30	26
	(F)			473 (5)	90 (5)	218 (5)	128 (3)	(0.40)		(7.3)		
AlO	(Al)	2.0015 (3)	2.0004 (3)	872 (1)	713 (1)	766 (2)	53.0 (7)	(20)[g]		(64)[g]	43	38
MgF	(F)	2.0020 (5)	2.0010 (5)	331 (3)	143 (3)	206 (3)	63 (2)	(0.39)		(3.6)		
SiO^+	(^{29}Si)	2.0012 (2)	2.0000 (2)	−924 (1)	−733 (1)	−797 (1)	−64 (1)	(17)[g]		(56)[g]		35

[a] A values in MHz. [b] % "s" and % "p" (valence orbitals) were calculated by the ratio of observed molecular values of A_{iso} and A_{dip}, respectively, to various neutral and charged atomic values of A_{iso} and A_{dip}. See notes *c–f* below. [c] Neutral Al A_{iso} and A_{dip} values used were 3911 and 83 MHz, respectively. Reference 24. [d] A_{iso} for Al^{2+} = 4590 MHz was calculated from a small basis set CI wave function—this investigation. [e] A_{dip} for Al^{2+} = 122 MHz was obtained from an SCF calculation—this investigation. [f] A_{dip} for Al^{2+} = 141 MHz was calculated by a charge correction method based on nuclear quadrupole results. See ref 26. [g] These free atom comparison method (FACM) results differ substantially from a detailed population analysis of a CI wave function which reproduces well the observed molecular values of A_{iso} and A_{dip}. See ref 8. Silicon neutral atomic values of A_{iso} and A_{dip} used were −4594 and −114 MHz, respectively.

tinuous irradiation from the neon resonance lamp produced AlF^+. During this photoionization deposition process the ejected electron is captured by neutral impurities in the neon lattice thereby creating an isolated and separated anion required for overall electroneutrality of the bulk matrix sample.

It is indeed fortunate that the neon discharge resonance lamp radiation at 16.8 eV does not significantly photobleach the sample. The reasons why this does not happen probably involve absorption of the resonant neon radiation by the neon matrix atoms which are present in large excess (10^6:1) and a greater production of cations by photoionization at this frequency than photoionization of the anions that are being created probably below the matrix surface. Observations supporting these suggestions include the following. After completing a given neon matrix deposition where ions (H_2O^+, N_2^+, CO^+, etc.) are formed by neon resonance photoionization, ESR signal strength is not reduced by additional irradiation at 16.8 eV with the neon resonance lamp. All reagent and neon matrix gases are not being deposited during this irradiation period which has been conducted for times as long as 1 h. The second observation is that irradiation of an already formed neon matrix containing all active reagents does not produce ion radicals detectable by ESR. In other words, irradiation must occur during the deposition process.

The reactive laser sputtering generation technique for producing molecules of interest in matrix isolation experiments might prove extremely useful for metal oxide and nitride molecules which have been difficult or impossible to form by other methods. We are currently investigating a wide range of chemical systems with this sputtering technique and plan to compare the results with similar FAB matrix (fast atom bombardment) experiments.[5] Niobium nitride, thought to be important in nuclear fusion vessels, is currently being investigated by laser sputtering. The authors (L.B.K.) are grateful to Professor Tom Dunn for pointing out that the electronic ground state of NbN^+ is probably $^2\Sigma$.

AlFX Impurity Species. For some of the high-temperature vaporization reduction reactions of AlF_3(s) with aluminum and calcium another charged radical was observed in the $g = 2$ area whose hyperfine pattern was a sextet of doublets. This species, which apparently contains one Al and one ^{19}F atom, was more noticeable on those vaporization experiments that used AlF_3(s) samples which had been less protected from atmospheric moisture. The laser sputtering experiments did not produce ESR spectra of this impurity radical. Evidence that this impurity species (as well as AlF^+) was an ion was obtained from the photobleaching effect described above. Only one geometric component of the ESR spectrum was sufficiently intense for analysis, and it exhibited a sextet hyperfine coupling constant of ≈331 G and doublet hf constant of ≈338 g. The line shape and slight deviations of these twelve observed line positions from exact axially symmetric line fitting equations seemed to indicate that the species was nonlinear. Our best guess at the identity of this charged impurity radical is $AlOF^+$. It is reasonable to assume that the third atom is oxygen since it could originate from hydrolysis reactions of AlF_3(s) and ^{16}O would not show ESR nuclear hfs. The doublet splitting is unusually large to be assigned to a hydrogen atom and Al seems to be the only reasonable choice to account for the sextet pattern.

In the early stages of these vaporization depositions and before conducting the laser sputtering experiments, we thought that this impurity species must be AlF^+ although in hindsight there were troublesome details in the ESR line fitting process that did not seem proper for an axially symmetric radical. After these initial experiments were completed, the extensive theoretical calculations of Davidson and Feller became available which predicted the Al hfs in the "real" AlF^+ radical to be approximately 920 G not 330 G. Subsequent vaporization experiments involving more careful handling of AlF_3(s) did show (in addition to this impurity radical) the presence of another radical whose identity is now clearly established as AlF^+ with $A_\perp$ = 994 (3) G and $A_\parallel$ = 1033 (3) G for its Al hfs. The theoretical results were definitely a compelling prompt to generate AlF^+ by an alternative and independent experimental method.

The possibility that the impurity radical could be $AlOF^+$ is interesting since this species has not been previously observed. Laser sputtering experiments on aluminum involving the simultaneous introduction of O_2 and F_2 are planned in order to produce a sufficiently intense ESR spectrum for detailed analysis. If this procedure is successful, it would be straightforward to utilize $^{17}O_2$ ($I = {}^5/_2$) for isotopic confirmation.

Discussion

Electron Structure of AlF^+ from ESR Data. The valence electronic structure of AlF^+ for the unpaired electron will be analyzed by different methods and compared with previous findings for the $^2\Sigma$ isoelectronic radicals AlO,[17] MgF,[18] and $^{29}SiO^+$.[8] The results of highly approximate methods commonly applied to ESR data for obtaining orbital occupancies and hybridization ratios will be compared with those of a Mulliken type population analysis conducted on an ab initio CI wave function that reproduces within 10% the observed molecular values of A_{iso} and A_{dip} for Al in the neon isolated AlF^+ radical.

Presented in Table II are the observed magnetic parameters for these diatomic radicals and the results of the free atom comparison method (FACM) for calculating % "s" and % "p" character utilizing neutral and charge corrected atomic Al values of A_{iso} and A_{dip}. The commonly applied set of atomic A_{iso} and A_{dip} parameters tabulated by Morton and Preston[24] for neutral Al yields 72% "3s" and 44% "3p_z" character; for ^{19}F the results are 0.40% "2s" and 7.3% "2p_z". Obviously, the total spin density of 124% obtained in this manner should be corrected for the extreme ionic character and formal charge that exists on Al in AlF^+.

Formal charge analysis of the CI wave function indicates that the charge is approximately −1 on fluorine and +2 on aluminum. The $Al^{2+}F^-$ model for AlF^+ readily accounts in a qualitative manner for the observed ESR nuclear hyperfine structure for both atoms. The Al($3s^23p^1$) ground state loses two electrons to form the ^{2}S state for $Al^{2+}(3s^1)$, and the near unit charge gained by fluorine produces a nearly closed shell (F^-) which should yield only small ^{19}F hfs in AlF^+. The observed nuclear hfs for Al (≈1000 G) in AlF^+ is the largest reported for any molecular Al radical, and the small ^{19}F hfs resembles closely the magnetic

(24) Morton, J. R.; Preston, K. F. *J. Magn. Reson.* **1978**, *30*, 577.

parameters observed for the highly ionic alkaline earth monofluoride neutral radicals (MgF, CaF, etc.) which can be described as M^+F^-. The large amount of Al $3s/3p_z$ hybridization that occurs is also consistent with previous MF radical studies.[18,25] Using an atomic A_{iso} value of 4590 MHz obtained from a small basis set CI calculation of Al^{2+} reduces the % "3s" character to 61% from 72% which was based on an Al neutral value of 3911 MHz.[24] Likewise, the % "$3p_z$" aluminum character is reduced from 44% for an Al neutral A_{dip} of 83 MHz[24] to 30% for an Al^{2+} A_{dip} of 122 MHz obtained from an SCF type calculation on the excited ^2P state of $Al^{2+}(3p^1)$. The reasonableness of this SCF A_{dip} calculation for Al^{2+} can be gauged by using an established procedure for correcting neutral atomic values of A_{dip} ($\langle r^{-3}\rangle$) for charge effects. The charge correction method described by Gordy[26] utilizing experimentally based correction factors for nuclear quadrupole results[27] yields an A_{dip} value for Al^{2+} of 141 MHz which agrees within 16% to the ab initio SCF calculation. This larger A_{dip} value for Al^{2+} yields a % "$3p_z$" character of 26% for AlF^+. Hence the sum of the individual orbital occupancies in AlF^+ is reduced from 124% to 95 or 99% depending upon which Al^{2+} A_{dip} parameter is chosen (the SCF value or the charged corrected neutral value). Therefore the FACM results utilizing charge corrected atomic values do produce a reasonable sum for the spin density based on the four independent experimental parameters of A_{iso} and A_{dip} for both Al and F.

Application of the negative charge correction to the ^{19}F neutral value of A_{dip} used in the above FACM analysis causes only a small increase in $2P_z$ character from 7% to 9%. Even this small amount of apparent open shell $2P_z$ character on fluorine cannot be accounted for by spin polarization effects alone. Therefore a small deviation from a full −1 charge on fluorine is indicated to account for the small degree of open shell $2P_z$ character reflected in the dipolar part of the ^{19}F hfs. Throughout these discussions A_{dip} and A_{iso} are defined in the following manner

$$A_{iso} = \tfrac{8}{3}\pi\, g_e g_n \beta_e \beta_n \langle \delta(r) \rangle$$

$$A_{dip} = \tfrac{1}{2} g_e g_n \beta_e \beta_n \left\langle \frac{3\cos^2\theta - 1}{r^3} \right\rangle$$

where all symbols have their standard definitions and the average is over the spin density.

Theoretical Calculations for AlF^+. Using an MCSCF wave function with a 6-orbital active space we obtained essentially the same equilibrium bond length (1.599 Å) as the PNO-CI/CEPA study of Klein and Rosmus.[21] The basis set consisted of the Dunning–Hay[28,29] double-ζ basis [11s,7p,2d/9s,5p,1d] contracted to [6s,4p,2d/4s,2p,1d] augmented with several sets of d functions. All possible excitations were allowed within the 6σ, 7σ, $2\pi_{x,y}$, and $3\pi_{x,y}$ orbitals. Although an experimental determination of the AlF^+ bond length has not been reported, Huber and Herzberg[30] report the bond lengths of several Rydberg excited states of AlF in the 1.596–1.598-Å range. The MCSCF geometry optimization was performed with GAMESS.[31]

A comparison of the AlF^+ HF and MCSCF wave functions revealed no significant differences such as were evident in the corresponding wave functions for AlO and SiO^+.[8] Presumably this is due to the much larger electronegativity of the fluorine cation than the oxygen atom, to use AlO as a comparison. Both at the HF and MCSCF levels of theory the fluorine gross atomic population is substantially greater than 9, indicating that the electron vacancy resides mostly on Al.

A larger (18s,12p,3d/12s,6p,2d) even-tempered primitive basis contracted to [12s,8p,3d/8s,4p,2d] was chosen for evaluating the hyperfine properties.[32] The d exponents (1.40, 0.39, and 0.11 on Al; 1.97 and 0.74 on F) were partially optimized at the SCF level. At the optimal geometry of the cation (1.599 Å) this basis yielded a neutral SCF energy of −341.4778 hartrees compared to a near HF limit value of −341.4832 hartrees at the optimal neutral geometry (1.654 Å).

Because an MCSCF calculation involving 86 basis functions and thousands of configurations is prohibitively large for the programs currently at our disposal, the CI property evaluations were performed with an alternative set of virtual orbitals, known as K orbitals,[33] which have been shown to closely mimic the frozen natural orbitals in cases where the HF configuration dominates the wave function. This, in turn, results in a more rapidly convergent CI expansion.

Properties were computed by using a CI wave function which consisted of all single and approximately 27 000 selected double excitations generated from the 10 space orbital products (25 spin-adapted configurations) listed in Table III. The selection of double excitations on the basis of their second-order energy

Table III. Orbital Occupancy of the Reference Configurations for AlF^+

	σ			π_x			π_y		
	6	7	8	1	2	3	1	2	3
1	2	1		2	2		2	2	
2	2	1		2	1	1	2	1	1
3	1	1	1	2	1	1	2	2	
4	1	1	1	2	2		2	1	1
5	2	1		2		2	2	2	
6	2	1		2	2		2		2
7	1	2		2	2		2	2	
8	1	2		2	2		2	1	1
9	1	2		2	1	1	2	2	
10	2	1	1	2	2		2	1	1

Table IV. Total Energies and Selected One-Electron Properties for AlF^+ with use of the (18s,12p,3d/12s,6p,2d) → [12s,8p,3d/8s,4p,2d] Basis

	SCF[a]		MRSD–CI[b]	
properties	Al	F	Al	F
isotropic hyperfine[c]	2298	165	2572	197
	(2343)[d]	(170)	(2622)	(203)
anisotropic hyperfine[c]	63	114	73	188
electric field gradient[e]	−1.33	0.62	−1.29	0.60
nuclear quad. coupling[f]	−46.9		−45.5	
Mulliken spin pop.				
(3s)	0.77		0.74	
(3pz)	0.17		0.18	
(2pz)	0.01	0.03	0.01	0.03

dipole moment = 2.35 D (origin = Al, F along the −z direction)

[a] The SCF energy with this basis is −341.1643 hartrees. [b] The CI energy was −341.5947 hartrees. There were 27 383 spin-adapted configurations selected from 2 767 230 generated. [c] Hyperfine parameters are given in units of MHz. The conversion factors used for converting δ in atomic units to a(iso) are the following: 139.1 (^{27}Al), 179.2 (^{19}F). The conversion factors for converting $(3z^2 - r^2)/r^5$ to a(aniso) are the following: 139.1 (^{27}Al), 502.2 (^{19}F). Note: the theoretical anisotropic results listed in this table correspond to $2A_{dip}$ where A_{dip} is defined in the text discussion of the experimental ESR results. [d] The isotropic values in parentheses have been scaled by the ratio (HF density at the nucleus—exact)/(HF density at the nucleus—this basis) in order to approximately account for the basis set deficiencies. [e] The electric field gradient is given in atomic units. [f] The nuclear quadrupole coupling constants are given in MHz and are defined as eqQ/h.

(25) Knight, L. B., Jr.; Mouchet, A.; Beaudry, W. T.; Duncan, M. *J. Mag. Reson.*, **1978**, *32*, 383.
(26) Gordy, W. *Theory and Applications of Electron Spin Resonance*; Wiley and Sons: New York, 1980; p 257.
(27) Townes, C. H.; Schawlow, A. L. *Microwave Spectroscopy*; McGraw-Hill: New York, 1955; p 239.
(28) Dunning, T. H., Jr. *J. Chem. Phys.* **1970**, *53*, 2823.
(29) Dunning, T. H., Jr.; Hay, P. J. *Methods of Electronic Structure Theory*; Schaefer, H. F., III, Ed.; Plenum: New York, 1977; p 23.
(30) Huber, K. P.; Herzberg, G. *Constants of Diatomic Molecules*; Van Nostrand-Reinhold Co.: New York, 1979.
(31) Dupvis, M.; Spangler, D.; Wendoloski, J. J.; *NRCC Software Catalog*, Vol. 1, Program GG01 (GAMESS), 1980.
(32) Schmidt, M. W.; Ruedenberg, K. *J. Chem. Phys.* **1981**, *71*, 3951.
(33) Feller, D.; Davidson, E. R. *J. Chem. Phys.* **1981**, *84*, 3977.

contributions was necessary due to the fact that in excess 3.8 million are possible. An estimated 91% of the MR SD–CI correlation energy was variationally recovered. Total energies and selected one-electron properties for AlF^+ are listed in Table IV. The CI calculated A_{dip} and A_{iso} values for Al of 36.5 and 2572 MHz, respectively, show excellent agreement with the observed values of A_{dip} = 37 (5) MHz and A_{iso} = 2819 (6) MHz. (See Table II.) The CI value of A_{iso} = 2622 MHz which has been scaled to correct for basis set deficiencies shows even closer agreement with experiment. (See Table IV.) The CI calculated values of A_{iso} = 197 MHz and A_{dip} = 94 MHz for ^{19}F hfs also show reasonable agreement with neon matrix experimental results of A_{iso} = 218 (5) MHz and A_{dip} = 128 (3) MHz for the AlF^+ radical.

The Mulliken population analysis of the AlF^+ wave functions was conducted in the manner described in the SiO^+ report.[8] Since the populations for the various valence orbitals of AlF^+ were obtained from ab initio wave functions which yield nuclear hyperfine parameters in excellent agreement with experiment, it is especially interesting to compare these theoretical populations with experimental populations obtained from the commonly applied free atom comparison method (FACM) discussed in the previous section. The FACM results utilizing the charge corrected neutral atomic values of A_{iso} and A_{dip} compare with the theoretical populations in the following manner (theoretical CI populations are underlined):

$$\text{Al"3s"}\ \underline{73}\%\ \text{vs.}\ 61\%;\ \text{Al"3p}_z\text{"}\ \underline{18}\%\ \text{vs.}\ 26\%$$

$$\text{F"2s"}\ \approx\underline{0}\%\ \text{vs.}\ 0.40\%;\ \text{F"2p}_z\text{"}\ \underline{3}\%\ \text{vs.}\ 9\%$$

The reasonable agreement between these two very different methods of obtaining orbital occupancies for AlF^+ should be contrasted with a similar comparison for the 3s and $3p_z$ orbitals of Si in $^{29}SiO^+$. The ESR FACM results for SiO^+ of 17% "s" and 56% "p_z" (based on neutral atomic Si parameters) differ substantially from the theoretical populations of 30% "s" and 27% "p_z" which were also obtained from a CI wave function yielding A_{iso} and A_{dip} values for ^{29}Si within 10% of the neon matrix experimental results. The source of the different results for the two methods in the SiO^+ case has been analyzed in detail and found to result from core–other valence overlap effects.[8] This type of inner-shell effect is not the result of spin polarization. For these types of diatomics the largest contributor to the core–other valence overlap effect comes from the overlap of the p_z orbital on the nonmetal atom. In AlF^+, the $2p_z$ spin density on F is approximately 10 times less than the $2p_z$ spin density on O in SiO^+. This major difference in the electronic structure of these two isoelectronic $^2\Sigma$ radicals accounts for the approximate agreement of experimental (FACM) and theoretical populations for AlF^+ and the large disagreement for SiO^+. The information gained in these studies should aid in distinguishing between those radicals that can be analyzed by the simple FACM approach and those that require more extensive theoretical analysis.

Electronic Ground State and g Tensor. AlF^+ has not been previously observed by any spectroscopic method. However, the observed **g** tensor and the theoretical calculations discussed above clearly indicate that the electronic ground state is $^2\Sigma$.

Since the observed values of $\Delta g_\parallel$ and $\Delta g_\perp$ ($\Delta g_\perp = g_\perp - g_e$) for AlF^+ are so small, only qualitative information can be obtained. The magnetic parameters for the $^2\Sigma$ isoelectronic series AlF^+, MgF, AlO, and SiO^+ presented in Table II reveal very similar g values. The values for $\Delta g_\parallel$ probably reflect only small neon matrix shifts since theory indicates that $\Delta g_\parallel$ would be zero in a first-order analysis. The small negative value of $\Delta g_\perp$ for AlF^+ indicates that spin–orbit coupling between the ground $^2\Sigma$ state and a regular $^2\pi$ excited state is dominant.[8] This $^2\pi_r$ state is probably best described as an Al $3p_\pi$ orbital. Hence a small amount of spin–orbit coupling between Al $3p_z$ in the ground electronic state and Al $3p_\pi$ in an excited $^2\pi_r$ would readily account for the observed $g_\perp$ value of 2.0000 (5). An accurate prediction of the location of this excited $2\pi_r$ state based on **g** tensor data alone cannot be made for AlF^+ given the small value of $\Delta g_\perp$.

Conclusion

The AlF^+ radical cation has been studied experimentally for the first time and found to have a $^2\Sigma$ ground state. Both laser sputtering and high-temperature vaporization methods were used for generating AlF(g) which was photoionized during neon matrix deposition experiments at 4 K. The laser-induced gas-metal reaction technique developed for this AlF^+ study should have widespread applications for other matrix investigations of reactive intermediates.

The magnetic parameters of AlF^+ in a neon matrix were determined by ESR and showed excellent agreement with those calculated by ab initio theoretical methods. The electronic structure of AlF^+ was compared with the isoelectronic $^2\Sigma$ radicals AlO, MgF, and SiO^+. Orbital populations for the unpaired electron were obtained from the commonly applied free atom comparison method (FACM) and from a Mulliken type population analysis of a CI wave function which yielded A_{iso} and A_{dip} values in close agreement with experiment. Population results from these two independent methods showed reasonable agreement in the case of AlF^+ but not for SiO^+. This difference was attributed to a large "core–other valence overlap effect" in SiO^+ that was not significant in the AlF^+ case since the spin density on the F $2p_z$ was approximately 10% that of the spin density on the O $2p_z$ in SiO^+. These findings should help predict those radical types which are inappropriate for the simple FACM analysis of ESR data.

Acknowledgment. Support from the National Science Foundation (CHE-8508085) and the Camille and Henry Dreyfus Foundation is gratefully acknowledged (L.B.K.). Part of the theoretical analysis was supported by a grant from the National Science Foundation (E.R.D.). A Dana Foundation undergraduate research scholarship is also gratefully acknowledged.